

ADMM-IDNN: Group-prior based Iteratively Double-reweighted Nuclear Norm Algorithm for Compressed Imaging via ADMM

Yunyi Li¹, Fei Dai², Yu Zhao², Xiefeng Cheng¹, and Guan Gui^{2,*}

¹ College of Electronic and Optical Engineering & College of Microelectronics, Nanjing University of Posts and Telecommunications, Nanjing 210023, China;

² College of Telecommunications & Information Engineering, Nanjing University of Posts and Telecommunications, Nanjing 210023, China

*Correspondence Author: guiguan@njupt.edu.cn

Abstract: Group-prior based regularization method has led to great successes in various image processing tasks, which can usually be considered as a low-rank matrix minimization problem. As a widely used surrogate function of low-rank, the nuclear norm based convex surrogate usually lead to over-shrinking phenomena, since the nuclear norm shrinks the rank components (singular value) simultaneously. In this paper, we propose a novel Group-prior based nonconvex image compressive sensing (CS) reconstruction framework via a family of nonconvex nuclear norms functions which contain common concave and monotonically properties. To solve the resulting nonconvex nuclear norm minimization (NNM) problem, we develop a Group based iteratively double-reweighted nuclear norm algorithm (IDNN) via an alternating direction method of multipliers (ADMM) framework. Our proposed algorithm can convert the nonconvex nuclear norms optimization problem into a double-reweighted singular value thresholding (DSVT) problem. Extensive experiments demonstrate our proposed framework achieved favorable reconstruction performance compared with current state-of-the-art convex methods.

Keywords: Group; low-rank; nonconvex; nuclear norm; double-reweighted; singular value thresholding; super-gradient.

I. Introduction

Image compressive sensing (CS) reconstruction [1] is a classic topic in low-level vision task, which has been widely studied in last decade. The goal of CS is to reconstruct a high-quality image or sequence \mathbf{X} from a small number of random measurements \mathbf{Y} , and one of the main technical challenges for CS is how to reduce the measurements whereas obtain high-quality images. Typical applications of CS include radar imaging [2,3], channel estimation in communications systems [4–8], signal detection [9–13], electrocardiogram signal reconstruction [14], magnetic resonant imaging (MRI) [15–17], and especially in image processing [18–20].

The reconstruction of high-quality images from a small number of measurements is a typical ill-posed inverse problem, it is well-known that the prior knowledge and sparse representation

model on image structures play a vital role in the CS reconstruction task. Exploiting more prior knowledge for minimization is often at the core in image CS reconstruction problem. In the past several years, the sparsity-based regularization methods have achieved great success in various CS applications. According to the sparse representation theory, every image can be represented accurately by a few dominant elements in a proper dictionary, which can be learned from natural images or prespecified. Traditional CS recovery approaches use the sparsity of an entire image in a predefined domain and the local structural patterns, such as the famous total-variation (TV) regularization [21]. However, these methods can only exploit a small number of structural features and some important artifacts will appear, e.g., texture and edge information, and thus these methods hard to improve reconstruction quality considerably.

As another classic image prior knowledge, recent work has revealed that the non-local similarity of patches can improve the reconstruction quality significantly by exploiting the nonlocal similarity features. For example, the well-known non-local mean filter [22], the promising denoiser BM3D [23], and the standard way for image recovery [24][25]. Recently, a state-of-the art sparse model of non-locally centralized sparse representation (NCSR) [26] is proposed for image restoration, which first obtain an accurate sparse coefficient vector, and then centralized the sparse coefficients to enhance the sparsity and improve the performance. Recent advances also suggest that the group-based approaches can often leads to great improvements by removing the artifacts and preserving the details. Since the Group is constructed using patches with similar structures, the rank of the Group is low, and the low-rank is a useful image prior [27].

For dealing with the image CS reconstruction problem, another important issue is how to regularize the sparsity. Conventional methods use the L_1 -norm as the surrogate of the L_0 -norm, and the resulting convex optimization problem can be easily solved. However, the achieved solution by L_1 -norm regularization is usually suboptimal to the L_0 -norm based minimization because of this loose appropriation. Hence, to appropriate the L_0 -norm by nonconvex function will achieve a more accurate solution [28]. Typical nonconvex surrogate function including L_p -norm [29–31], Smoothly Clipped Absolute Deviation (SCAD) [32], Logarithm [33], and Minimax Concave Penalty (MCP) [34], etc.. Recently, the low-rank based regularization approaches have shown its great potentials in image processing [35][36], especially in CS-based image recovery [37][38]. It is the fact that the adjacent patches in an image have the similar structures, if several similar patches are constructed as a group matrix, then the matrix shows the low-rank property. Hence, the image CS problem can convert into a low-rank matrix approximation problem. Since the low-rank minimization problem is a NP-hard problem, it is usually relaxed as the nuclear norm minimization (NNM) problem [27]. The idea of low-rank is based on the sparsity of a matrix singular values. Like the L_0 -norm based regularization, the low-rank based minimization problem is also a NP-hard problem, which is usually relaxed to the convex nuclear norm.

In this paper, inspired by the successes of nonconvex regularization approaches and the group-prior model, we extend a family of typical nonconvex surrogate penalties of L_0 -norm on singular values of the group matrix to enhance the low-rank reconstruction performance. We first connect Group-prior with a family of nonconvex nuclear norms for image CS problem, in which, the local sparsity and nonlocal similarity of image can be unified simultaneously in a non-convex framework. Second, to make the proposed model more robust and tractable, we develop an alternative direction method of multipliers (ADMM) framework for our non-convex minimization problem. Third, we propose a Group prior based iteratively double-reweighted nuclear norm (IDNN) algorithm to solve

the resulting nonconvex optimization sub-problem. Our proposed IDNN algorithm consists of two stage: we first develop a iteratively reweighted nuclear norm (IRNN) algorithm by observing that all gradients of nonconvex surrogate function are nonnegative and monotonically increasing in $[0, \infty)$, and then proposed a double-reweighted strategy to avoid the over-shrinking on each singular values. At last, we evaluate the proposed nonconvex framework by using several well-known nonconvex penalty functions of logarithm, MCP and SCAD on the classic image CS reconstruction problem.

The remainder of this paper is as follows. In the second section, we will review the group-prior theory and develop a Group-prior based image CS reconstruction framework via a family of nonconvex nuclear norm functions. In the section III, we will propose our iteratively double-reweighted nuclear norm algorithm via ADMM strategy. Section IV provides simulation results compared with current state-of-the-art methods to demonstrate the effectiveness and priority of our proposed framework. Finally, a brief summary will be concluded in section V.

II. Group-prior based Nonconvex Nuclear Norm Framework for Image CS Reconstruction

Traditional patch-based sparse representation modeling is inaccurate, because each patch is considered separately and the relationship among patches is ignored. The new group-prior based model can represent the image in the domain of group, which not only enhances intrinsic local sparsity, but also enhances the nonlocal similarity simultaneously [27]. This section will first develop a Group-prior based Image CS Reconstruction framework via low-rank minimization, which benefits from the low-rank property of each group, and then propose a nonconvex nuclear norm framework to enhance the low-rank reconstruction performance by extending a family of typical nonconvex surrogate penalties on singular values of the group matrix.

2.1. Group-prior based Image CS Reconstruction via low-rank minimization

For every original image $\mathbf{X} \in \mathbb{R}^{\sqrt{N} \times \sqrt{N}}$, which can be divided into n overlapped patches $\mathbf{X}_k, k = 1, 2, \dots, n$ with the size of $\sqrt{\mathcal{B}_c} \times \sqrt{\mathcal{B}_c}, \mathcal{B}_c < N$. Given a searching window with the size of $L \times L$ for each patch \mathbf{X}_k , its c best matched patches will be searched using the well-known Euclidean distance as the similarity criterion, and the set of these best similar patches denotes $S_{\mathbf{x}_k}$. Next, its c best matched patches are stacked into a matrix with the size of $\mathcal{B}_c \times c$, denoted by $\mathbf{X}_{G_k} = [\mathbf{X}_{G_k,1}, \mathbf{X}_{G_k,2}, \dots, \mathbf{X}_{G_k,c}] \in \mathbb{R}^{\mathcal{B}_c \times c}$, where each patch can be vectorized as $\mathbf{X}_{G_k,i} \in \mathbb{R}^{\mathcal{B}_c \times 1}, i = 1, 2, \dots, c$ as the columns. Such matrix \mathbf{X}_{G_k} with c patches containing similar structures is named as group, we define the construction process of group as $\mathbf{X}_{G_k} = G_k(\mathbf{X})$, where the operator $G_k(\cdot)$ denotes the group construction operator from \mathbf{X} . Different from the traditional patch-based sparse representation model, the GSR model can exploit the nonlocal self-similarity and enhance the local sparsity by using the group as basic unit for sparse representation.

In general, the image compressive sensing observation model can be expressed as

$$\mathbf{Y} = \mathbf{H}\mathbf{X} + \mathbf{n} \quad (1)$$

where \mathbf{H} denotes the random projection matrix with the size of $M \times N, (M < N)$, \mathbf{X} and \mathbf{n} are the desired image and the additive noise. Suppose the original image $\mathbf{X} \in \mathbb{R}^N$ (also $\mathbf{X} \in \mathbb{R}^{\sqrt{N} \times \sqrt{N}}$) can be sparse in the certain basis or domain Ψ , denotes as $\alpha = \Psi^T \mathbf{X}$. Based on the CS theory, if

the measurement matrix \mathbf{H} satisfies the so called restricted isometry property (RIP) [1], then the CS reconstruction problem can be resolved by the following regularization method

$$\hat{\mathbf{X}} = \arg \min_{\mathbf{X}} \frac{1}{2} \|\mathbf{Y} - \mathbf{H}\mathbf{X}\|_2^2 + \lambda \cdot R(\Psi^T \mathbf{X}) \quad (2)$$

where $R(\cdot)$ denotes regularization term, e.g., L_1 -norm, which measures the sparsity degree of image in the domain Ψ , and can provide the necessary prior knowledge for minimization, the regularization parameter λ control the tradeoff between the fidelity term and the regularization term.

Accordingly, after stacking the related similar patches to generate the group $\mathbf{X}_{G_k} \in \mathbb{R}^{B_s \times c}$, $k = 1, 2, \dots, n$, each group \mathbf{X}_{G_k} containing the patches with similar structures, hence, the matrix \mathbf{X}_{G_k} has a low-rank property. By incorporating the low-rank prior for CS reconstruction problem, the optimization problem (2) can be turned into the following matrix low-rank minimization problem

$$\hat{\mathbf{X}} = \arg \min_{\mathbf{X}} \frac{1}{2} \|\mathbf{Y} - \mathbf{H}\mathbf{X}\|_2^2 + \lambda \sum_{k=1}^n \text{Rank}(\mathbf{X}_{G_k}) \quad (3)$$

where $\text{Rank}(\mathbf{X}_{G_k})$ is the rank of matrix \mathbf{X}_{G_k} .

2.2. Modeling of nonconvex nuclear norm framework

Considering the following low rank matrix recovery problem

$$\tilde{\mathbf{X}} = \arg \min_{\mathbf{X}} \frac{1}{2} \|\mathbf{Y} - \mathbf{A}(\mathbf{X})\|_F^2 + \lambda \text{Rank}(\mathbf{X}) \quad (4)$$

where the operator $\mathbf{A}(\cdot)$ denotes the linear mapping, \mathbf{Y} can be an observation matrix or vector with the size of $\mathbf{A}(\mathbf{X})$, and $\|\cdot\|_F$ presents the Frobenius norm. It is often a challenge problem to solve the above low rank optimization problem (9) and the rank function is usually relaxed as the convex nuclear norm, $\|\mathbf{X}_{G_k}\|_* = \sum_i |\sigma_i(\mathbf{X})|$, where $\sigma_i(\mathbf{X})$ denotes the singular values of matrix \mathbf{X} .

Same to the above low rank minimization problem, the low-rank based image CS reconstruction problem (4) is a NP-hard problem, after replacing by the popular convex nuclear norm, the NNM based optimization problem can be expressed as

$$\hat{\mathbf{X}} = \arg \min_{\mathbf{X}} \frac{1}{2} \|\mathbf{Y} - \mathbf{H}\mathbf{X}\|_2^2 + \lambda \sum_{k=1}^n \|\mathbf{X}_{G_k}\|_* \quad (5)$$

where $\|\mathbf{X}_{G_k}\|_* = \sum_i |\sigma_i(\mathbf{X}_{G_k})|$ denotes the nuclear norm, and $\sigma_i(\mathbf{X}_{G_k}), i = 1, 2, \dots, d, d = \min(B_s, c)$ are the singular values of matrix \mathbf{X}_{G_k} . Although the above model (5) can incorporate the low rank prior knowledge, the NNM usually treat different rank components (singular values) equally and simultaneously, hence it cannot achieve the approximation of the low-rank accurately. Recently, the nonconvex penalized regularization methods have shown great potential to improve the sparse recovery performance, typical nonconvex surrogate function include the L_p function [30], Smoothly Clipped Absolute Deviation (SCAD) [32], Logarithm function [33], and Minimax Concave Penalty (MCP) [34], etc.. Accordingly, the nonconvex NNM can improve the convex surrogates based minimization effectively. In this paper, we employ a class of nonconvex functions to regularize the sparsity, then our proposed image compressive sensing reconstruction framework can be expressed as

$$\hat{\mathbf{X}} = \arg \min_{\mathbf{X}} \frac{1}{2} \|\mathbf{Y} - \mathbf{H}\mathbf{X}\|_2^2 + \lambda \cdot \sum_{k=1}^n \sum_{i=1}^{\min(B_s, c)} g(\sigma_i(\mathbf{X}_{G_k})) \quad (6)$$

where $\sigma_i(\mathbf{X}_{G_k})$ is the i -th singular value of $\mathbf{X}_{G_k} \in \mathbb{R}^{B_s \times c}$, $g(\cdot)$ denotes the nonconvex penalty functions. For our proposed nonconvex framework, some classic nonconvex surrogate functions of $\|\boldsymbol{\theta}\|_0$ are detailed as the **definition 1**.

Definition 1 Popular and typical nonconvex surrogate function of the $\|\boldsymbol{\theta}\|_0$:

(1) the L_p function [30]:

$$L_p(\theta, p) = \lambda \theta^p. \quad (7)$$

(2) the smoothly clipped absolute deviation (SCAD) function [32]:

$$SCAD(\theta, \gamma, \lambda) = \begin{cases} \lambda \theta, & \text{if } \theta \leq \lambda \\ \frac{-\theta^2 + 2\gamma\lambda\theta - \lambda^2}{2(\gamma-1)}, & \text{if } \lambda < \theta \leq \gamma\lambda \\ \frac{\lambda^2(\gamma+1)}{2}, & \text{if } \theta > \gamma\lambda \end{cases}. \quad (8)$$

(3) the logarithm function [33]:

$$Logarithm(\theta, \gamma) = \frac{\lambda}{\log(\gamma+1)} \log(\gamma\theta + 1). \quad (9)$$

(4) the minimax concave penalty (MCP) function [34]:

$$MCP(\theta, \gamma, \lambda) = \begin{cases} \lambda\theta - \frac{\theta^2}{2\gamma}, & \text{if } \theta < \gamma\lambda \\ \frac{\gamma\lambda^2}{2}, & \text{if } \theta > \gamma\lambda \end{cases}. \quad (10)$$

(5) the laplace function [39]:

$$Laplace(\theta) = \lambda \left(1 - e^{-\frac{\theta}{\gamma}}\right). \quad (11)$$

(6) the exponential-type penalty (ETP) function [40]:

$$ETP(\theta) = \frac{\lambda}{1-e^{-\gamma}} (1 - e^{-\gamma\theta}). \quad (12)$$

(7) the capped L_1 function :

$$Capped L_1(\theta) = \begin{cases} \lambda\theta, & \text{if } \theta < \gamma \\ \lambda\gamma, & \text{if } \theta \geq \gamma\lambda \end{cases}. \quad (13)$$

(8) the geman function:

$$Geman(\theta) = \frac{\lambda\theta}{\theta+\gamma}. \quad (14)$$

III. Iteratively Double-reweighted Nuclear Norm Algorithm

To solve the nonconvex optimization problem (6), we propose a Group prior based iteratively double-reweighted nuclear norm (IDNN) algorithm which consists of three stages: Firstly, the alternative direction method of multipliers (ADMM) framework is applied to our non-convex minimization problem. Secondly, we develop an iteratively reweighted nuclear norm (IRNN) algorithm for the \mathbf{X}_G -subproblem by observing that all gradients of nonconvex surrogate function are nonnegative and monotonically increasing in $[0, \infty)$. Thirdly, the double-reweighted strategy is utilized to avoid the over-shrinking on each singular value.

3.1 ADMM framework for Group-prior based nonconvex nuclear norm model

The alternative direction method of multipliers (ADMM) framework is an efficient and effective approach for large-scale optimization problem, which can split the constrained minimization problem into several constrained sub-problems, and thus only using a small memory footprint [41]. In the first stage, we first considering the optimization model (6), by introducing the auxiliary variable \mathbf{Z} , then

$$\mathbf{X} = \arg \min_{\mathbf{X}} \frac{1}{2} \|\mathbf{Y} - \mathbf{H}\mathbf{X}\|_2^2 + \lambda \cdot \sum_{k=1}^n \sum_{i=1}^{\min(B_s, c)} g(\sigma_i(\mathbf{X}_{G_k})), \text{ s. t. } \mathbf{Z} = \mathbf{X}. \quad (15)$$

Then we have the following three iterative steps

$$\mathbf{Z}^{(t+1)} = \arg \min_{\mathbf{Z}} \frac{1}{2} \|\mathbf{Y} - \mathbf{H}\mathbf{Z}\|_2^2 + \frac{\mu}{2} \|\mathbf{Z} - \mathbf{X}^{(t)} - \mathbf{W}^{(t)}\|_2^2, \quad (16)$$

$$\mathbf{X}^{(t+1)} = \arg \min_{\mathbf{X}} \frac{\mu}{2} \|\mathbf{Z}^{(t+1)} - \mathbf{X} - \mathbf{W}^{(t)}\|_2^2 + \lambda \cdot \sum_{k=1}^n \sum_{i=1}^{\min(B_s, c)} g(\sigma_i(\mathbf{X}_{G_k})), \quad (17)$$

$$\mathbf{W}^{(t+1)} = \mathbf{W}^{(t)} - (\mathbf{Z}^{(t+1)} - \mathbf{X}^{(t+1)}). \quad (18)$$

Then the optimization problem (15) can be split into two sub-problems (16) and (17).

(A). \mathbf{Z} -subproblem

The \mathbf{Z} -subproblem of (16) is a strictly convex minimization problem, which has a closed-form solution expressed as

$$\mathbf{Z} = (\mathbf{H}^T \mathbf{H} + \mu \mathbf{I})^{-1} (\mathbf{H}^T \mathbf{Y} + \mu (\mathbf{X} + \mathbf{W})) \quad (19)$$

where \mathbf{I} denotes the identity matrix. It is often inefficient to achieve the solution by (19) directly for CS reconstruction problem, since without specific structure of observation matrix \mathbf{H} . To avoid the computing of matrix inverse, here, we employ the gradient descent method to solve the sub-problem of (19) by [27]

$$\tilde{\mathbf{z}} = \mathbf{Z} - \eta \mathbf{d} \quad (20)$$

where the parameter η is the optimal step, \mathbf{d} denotes the gradient direction of $\frac{1}{2} \|\mathbf{Y} - \mathbf{H}\mathbf{Z}\|_2^2 + \frac{\mu}{2} \|\mathbf{Z} - \mathbf{X} - \mathbf{W}\|_2^2$, then we have

$$\mathbf{d} = \mathbf{H}^T \mathbf{H}\mathbf{Z} - \mathbf{H}^T \mathbf{Y} + \mu (\mathbf{Z} - \mathbf{X} - \mathbf{W}). \quad (21)$$

(B). \mathbf{X}_G -subproblem

After achieving \mathbf{Z} , the \mathbf{X}_G -subproblem can be expressed as

$$\mathbf{X} = \arg \min_{\mathbf{X}} \frac{\mu}{2} \|\mathbf{R} - \mathbf{X}\|_2^2 + \lambda \cdot \sum_{k=1}^n \sum_{i=1}^{\min(B_s, c)} g(\sigma_i(\mathbf{X}_{G_k})) \quad (22)$$

where $\mathbf{R}^{(t)} = \mathbf{Z}^{(t)} - \mathbf{W}^{(t-1)}$. The problem of (22) is a typical denoising problem, where \mathbf{R} denotes the noisy observation of \mathbf{X} [38]. However, it is difficult to solve the problem (22) because of the complicated structure of the regularizer. By grouping the similar patches to generate the $\mathbf{R}_{G_k} \in \mathbb{R}^{B_c \times c}$, according to the relationship between $\sum_{k=1}^n \|\mathbf{R}_{G_k} - \mathbf{X}_{G_k}\|_2^2$ and $\|\mathbf{R} - \mathbf{X}\|_2^2$, then we have [42]

$$\|\mathbf{R} - \mathbf{X}\|_2^2 = \frac{N}{K} \sum_{k=1}^n \|\mathbf{R}_{G_k} - \mathbf{X}_{G_k}\|_2^2 \quad (23)$$

where $K = n \times c \times B_s$. Then the problem of (22) can be transformed into the following n subproblems

$$\hat{\mathbf{X}}_{G_k} = \arg \min_{\mathbf{X}_{G_k}} \frac{1}{2} \sum_{k=1}^n \left\{ \|\mathbf{R}_{G_k} - \mathbf{X}_{G_k}\|_2^2 + \tau \sum_{i=1}^{\min(B_s, c)} g(\sigma_i(\mathbf{X}_{G_k})) \right\} \quad (24)$$

where $\tau = \frac{\lambda K}{\mu N}$. For each group \mathbf{X}_{G_k} , we have

$$\hat{\mathbf{X}}_{G_k} = \arg \min_{\mathbf{X}_{G_k}} \frac{1}{2} \|\mathbf{R}_{G_k} - \mathbf{X}_{G_k}\|_2^2 + \tau \sum_{i=1}^{\min(B_s, c)} g(\sigma_i(\mathbf{X}_{G_k})). \quad (25)$$

3.2 Iterative reweighted algorithm for nonconvex nuclear norm minimization

This subsection will develop an iterative reweighted algorithm for nonconvex NNM problem (25). According to the **Definition 1**, we can observe that all nonconvex functions contain common properties: concave and monotonically increasing on $[0, \infty)$. We first give the definition of supergradient for all the nonconvex functions defined in (26) to (33).

Definition 2 The corresponding supergradient can be described as

(1) the supergradient of L_p

$$\partial(L_p(\theta, p)) = \begin{cases} \infty, & \text{if } \theta = 0 \\ \lambda p \theta^{p-1}, & \text{if } \theta > 0 \end{cases}. \quad (26)$$

(2) the supergradient of Smoothly Clipped Absolute Deviation (SCAD)

$$\partial(\text{SCAD}(\theta, \gamma, \lambda)) = \begin{cases} \lambda, & \text{if } \theta = 0 \\ \frac{\gamma\lambda - \theta}{\gamma - 1}, & \text{if } \lambda < \theta \leq \gamma\lambda \\ 0, & \text{if } \theta > \gamma\lambda \end{cases}. \quad (27)$$

(3) the supergradient of Logarithm

$$\partial(\text{Logarithm}(\theta, \gamma)) = \frac{\gamma\lambda}{(\gamma\theta + 1) \log(\gamma + 1)}. \quad (28)$$

(4) the supergradient of Minimax Concave Penalty (MCP)

$$\partial(\text{MCP}(\theta, \gamma, \lambda)) = \begin{cases} \lambda - \frac{\theta}{\gamma}, & \text{if } \theta < \gamma\lambda \\ 0, & \text{if } \theta \geq \gamma\lambda \end{cases}. \quad (29)$$

(5) the supergradient of Laplace

$$\partial(\text{Laplace}(\theta)) = \frac{\lambda}{\gamma} e^{-\frac{\theta}{\gamma}}. \quad (30)$$

(6) the supergradient of Exponential-Type Penalty (ETP)

$$\partial(\text{ETP}(\theta)) = \frac{\lambda\gamma}{1 - e^{-\gamma}} e^{-\gamma\theta}. \quad (31)$$

(7) the supergradient of Capped L_1

$$\partial(\text{Capped } L_1(\theta)) = \begin{cases} \lambda, & \text{if } \theta < \gamma \\ [0, \lambda], & \text{if } \theta = \gamma \\ 0, & \text{if } \theta \geq \gamma\lambda \end{cases}. \quad (32)$$

(8) the supergradient of Geman

$$\partial(\text{ETP}(\theta)) = \frac{\lambda\gamma}{(\theta + \gamma)^2}. \quad (33)$$

We can easily observe that their super-gradients are nonnegative and monotonically decreasing, thus we can propose a general solver for the problem (25).

Lemma 1. [43] Let $g: \mathbb{R}^n \rightarrow \mathbb{R}$ be concave, if for every $\mathbf{y} \in \mathbb{R}^n$, a vector \mathbf{v} is a super-gradient of $g(\mathbf{x})$ at the point $\mathbf{x} \in \mathbb{R}^n$, then

$$g(\mathbf{y}) \leq g(\mathbf{x}) + \langle \mathbf{v}, \mathbf{y} - \mathbf{x} \rangle. \quad (34)$$

Lemma 2. [43][44] For any $\lambda > 0$, $\mathbf{Y} \in \mathbb{R}^{M \times N}$, and the weighting vector $\tilde{\omega} = [\tilde{\omega}_1, \tilde{\omega}_2, \dots, \tilde{\omega}_s]$ with $0 \leq \tilde{\omega}_1 \leq \tilde{\omega}_2 \leq \dots \leq \tilde{\omega}_s$, ($s = \min(M, N)$), then the globally optimal solution of following optimization problem

$$\min \frac{1}{2} \|\mathbf{Y} - \mathbf{X}\|_F^2 + \lambda \sum_{i=1}^s \tilde{\omega}_i \sigma_i(\mathbf{X}) \quad (35)$$

is given by the weighted singular value thresholding (WSVT)

$$\mathbf{X}^* = \mathbf{U} \mathbf{S}_{\lambda \tilde{\omega}}(\mathbf{\Sigma}) \mathbf{V}^T \quad (36)$$

where $\mathbf{Y} = \mathbf{U} \mathbf{\Sigma} \mathbf{V}^T$ denotes the SVD of \mathbf{Y} , and for each diagonal element Σ_{ii} of $\mathbf{\Sigma}$, there is

$$\mathbf{S}_{\lambda \tilde{\omega}}(\mathbf{\Sigma}) = \text{Diag}\{(\Sigma_{ii} - \lambda \tilde{\omega}_i)_+\}. \quad (37)$$

In this paper, since the function of $g(\cdot)$ is concave on $[0, \infty)$, according to the **Definition 2** of the super-gradient, and the **Lemma 1**, we can have

$$g(\sigma_i(\mathbf{X}_{G_k})) \leq g(\sigma_i(\mathbf{X}_{G_k}^t)) + \tilde{\omega}_{k,i}^t (\sigma_i(\mathbf{X}_{G_k}) - \sigma_i(\mathbf{X}_{G_k}^t)) \quad (38)$$

where $\tilde{\omega}_{k,i}^t \in \partial [g(\sigma_i(\mathbf{X}_{G_k}^t))]$, termed as the first-reweight here. Since $\sigma_1(\mathbf{X}_{G_k}^t) \geq \sigma_2(\mathbf{X}_{G_k}^t) \geq \dots \geq \sigma_m(\mathbf{X}_{G_k}^t) \geq 0$, then according to the antimotone property of super-gradient defined in (26) – (33), we have

$$0 \leq \tilde{\omega}_{k,1}^t \leq \tilde{\omega}_{k,2}^t \leq \dots \leq \tilde{\omega}_{k,m}^t \quad (39)$$

where $\mathbf{X}_{G_k}^t$ denote the t -th iteration solution. Motivated by the property, the minimization problem (25) can be converted into the following relaxed problem by

$$\begin{aligned} \mathbf{X}_{G_k}^{t+1} &= \arg \min_{\mathbf{X}_{G_k}} \frac{1}{2} \|\mathbf{R}_{G_k} - \mathbf{X}_{G_k}\|_2^2 + \tau g(\sigma_i(\mathbf{X}_{G_k})) \\ &= \arg \min_{\mathbf{X}_{G_k}} \frac{1}{2} \|\mathbf{R}_{G_k} - \mathbf{X}_{G_k}\|_2^2 + \tau [g(\sigma_i(\mathbf{X}_{G_k}^t)) + \tilde{\omega}_{k,i}^t (\sigma_i(\mathbf{X}_{G_k}) - \sigma_i(\mathbf{X}_{G_k}^t))] \\ &= \arg \min_{\mathbf{X}_{G_k}} \frac{1}{2} \|\mathbf{R}_{G_k} - \mathbf{X}_{G_k}\|_2^2 + \tau \sum_{i=1}^m (\tilde{\omega}_{k,i}^t \sigma_i(\mathbf{X}_{G_k})) \end{aligned} \quad (40)$$

where $\tilde{\omega}_{k,i}^t \in \partial [g(\sigma_i(\mathbf{X}_{G_k}^t))]$ denotes the reweights for each singular value. The optimization of (40) can be effectively resolved by the following **Lemma 2**. Therefore, according to the **Lemma 2**, a close-form solution of (40) can be achieved as

$$\mathbf{X}_{G_k}^{t+1} = \mathbf{U}_{G_k} \mathbf{S}_{\lambda \tilde{\omega}_i^t}(\mathbf{\Sigma}_{G_k}) \mathbf{V}_{G_k}^T \quad (41)$$

where

$$\mathbf{S}_{\lambda \tilde{\omega}_i^t}(\mathbf{\Sigma}_{G_k}) = \text{Diag}\{(\varsigma_{k,i} - \tau \tilde{\omega}_{k,i}^t)_+\}, i = 1, 2, \dots, \min(B_s, c), \quad (42)$$

in which $(x)_+ = \max(x, 0)$, $\mathbf{\Sigma}_{G_k} = \text{diag}(\varsigma_{k,1}, \varsigma_{k,2}, \dots, \varsigma_{k, \min(B_s, c)})$, \mathbf{U}_{G_k} and $\mathbf{V}_{G_k}^T$ are achieved by the singular value decomposition (SVD) of \mathbf{R}_{G_k} , e.g., $\mathbf{R}_{G_k} = \mathbf{U}_{G_k} \mathbf{\Sigma}_{G_k} \mathbf{V}_{G_k}^T$. By iteratively updating the reweighting $\tilde{\omega}_{k,i}^t \in \partial [g(\sigma_i(\mathbf{X}_{G_k}^t))]$, the problem (25) can be resolved effectively.

3.4 Double-reweighted strategy for nonconvex nuclear norm minimization

In the second stage, the second-reweighted strategy is utilized to avoid the over-shrinking on each singular values. Based on the optimization model (6), we have connected the Group-prior with a family of nonconvex nuclear norms for image compressive sensing problem. According to the theory of low rank minimization, the rank of a certain matrix only corresponds to the larger nonzero singular values, what's more, larger singular values often contain more information of matrix. For better approximate the rank of the group-matrix, hence, the larger singular values should be shrank less, and the smaller ones should be shrank more. Inspired by the reweighted L_1 minimization [45], we propose a more flexible and effective reweight strategy for corresponding singular value $\sigma_i(\mathbf{X}_{G_k})$ to avoid over-shrinking, termed as the second-reweight here, it can be expressed as

$$\omega_{k,i} = \frac{1}{|\sigma_i(\mathbf{X}_{G_k})| + \varepsilon} \quad (43)$$

where $\sigma_i(\mathbf{X}_{G_k}) = (\boldsymbol{\Sigma}_{G_k})_i = \zeta_{k,i}$, $i = \min(B_s, c)$, and the small constant parameter ε can prevent the denominator from zero, e.g., 10^{-2} . Then our proposed double-reweighted strategy can avoid over-shrinking by weighting to each singular value effectively. Then the close-form solution (41) can be transformed into

$$\mathbf{X}_{G_k}^t = \mathbf{U}_{G_k} \mathbf{S}_{\lambda \omega_{ki} \tilde{\omega}_{k,i}^t}(\boldsymbol{\Sigma}_{G_k}) \mathbf{V}_{G_k}^T \quad (44)$$

where $\mathbf{S}_{\lambda \omega_{ki} \tilde{\omega}_{k,i}^t}(\boldsymbol{\Sigma}_{G_k}) = \text{Diag}\left\{\left((\boldsymbol{\Sigma}_{G_k})_{ii} - \tau \omega_{ki} \tilde{\omega}_{k,i}^t\right)_+\right\}$.

After achieving all $\hat{\mathbf{X}}_G$, $k = 1, 2, \dots, n$, then we can obtain the desired image by

$$\hat{\mathbf{X}} = \sum_{k=1}^n G_k^T(\hat{\mathbf{X}}_{G_k}) ./ \sum_{k=1}^n G_k^T(\mathbf{1}_{B_c}) \quad (45)$$

where the $G_k^T(\cdot)$ denotes the transpose grouping operator, which can reconstruct the original image from the group. It is the fact that these parameters play a key role for optimization, which can balance the fidelity term and the regularization term. To adaptively balance their relationship, we employ an adaptive scheme which based on the maximum a posterior [26], expressed as

$$\lambda = \frac{2\sqrt{2}\delta^2}{\theta + \varepsilon} \quad (46)$$

that is

$$\tau = \frac{2\sqrt{2}\delta^2\lambda K}{\mu N(\theta + \varepsilon)} \quad (47)$$

where δ^2 denotes the deviation of \mathbf{R}_{G_k} , and θ represents the variance of \mathbf{X}_{G_k} , the small positive constant ε will prevent the denominator from zero.

3.4 Summary of the IDNN Algorithm

The whole procedure of our proposed algorithm of IDNN can be shown in the **Algorithm 1**.

Algorithm 1 Proposed Iteratively Double-reweighted Nuclear Norm Algorithm (ADMM-IDNN)

Input: The Observation \mathbf{Y} , the compressed sampling matrix \mathbf{H} ;

Initialization: $c, \mathcal{B}_c, t = 0, \delta, \varepsilon, \mu, \gamma, \lambda^{(0)}, \mathbf{W}^{(0)} = \mathbf{0}, \mathbf{Z}^{(0)} = \mathbf{0}$;

Repeat

 Updating $\mathbf{Z}^{(t+1)}$ using the Eq. (20) (21);

 Computing $\mathbf{R}^{(t+1)} = \mathbf{Z}^{(t+1)} - \mathbf{W}^{(t)}$;

Constructing the groups $\{\mathbf{R}_{G_k}^{(t+1)}\}$ from $\mathbf{R}^{(t+1)}$;

Computing parameter $\tau = \frac{\lambda^{(t)}K}{\mu N}$;

for each group $\mathbf{R}_{G_k}^{(t+1)}$

Singular value decomposition by $\mathbf{R}_{G_k}^{(t+1)} = \mathbf{U}_{G_k} \mathbf{\Sigma}_{G_k} \mathbf{V}_{G_k}^T$ in (44);

Updating weightings $\omega_i^{(t+1)}$ by (43);

Updating the adaptive parameter $\lambda^{(t+1)}$ (46);

Reconstruct $\mathbf{X}_{G_k}^{(t+1)}$ using the Eq. (45);

end

Computing $\mathbf{X}^{(t+1)}$ by concatenating all the dictionaries $\{\mathbf{X}_{G_k}\}$;

Computing $\mathbf{W}^{(t+1)}$ using Eq. (23);

$t = t + 1$;

Until the maximum iteration number is reached.

Output: The reconstructed image $\mathbf{X}^{(t+1)}$.

IV. Experimental Results

In this section, we employ several classical cases of MCP, SCAD and logarithm function as surrogates to evaluate the performance of our proposed nonconvex framework for compressive sensing reconstruction tasks. Because of the original image \mathbf{X} is unknown, this paper employ the result of a state-of-the art algorithm MH [46] as initialization for our proposed framework. It is the fact that the parameters in **Algorithm 1** have great effects on the reconstructed performance, include the regularization parameter λ , the penalty factor μ , and the best number of patches c . We will first employ an adaptive scheme for updating the regularization parameter λ , and choose optimal values of μ and c by experiments. Then we analysis convergence of our proposed algorithm for the nonconvex optimization problem. To better illustrate the performance, we compare the performance of proposed algorithm with several state-of-the-art convex compressive sensing reconstruction algorithms. We introduce two metrics to evaluate the reconstruction performance of all algorithms, namely, the peak signal-to-noise ratio (PSNR) and the metric feature similarity (FSIM) [47]. All the natural images for experiments are listed in the Figure 1.



Figure 1 Nine typical 256×256 natural images for experiments: Barbara, Boats, Fingerprint, Foreman, House, Leaves, Monarch and Starfish.

4.1 Parameters setting

From the **Algorithm 1**, we can find that there are some important parameters, the regularization parameter λ , the penalty factor μ , and the optimal number of similar patch c , and other parameters,

such as the patch size of $\sqrt{B_c} \times \sqrt{B_c}$. Empirically, in this paper, we will set the block size as 32×32 , and the patch size is set to be 6×6 , and the searching window is set to be 20×20 for all the experiments. To evaluate the effects of other two parameters for the reconstructed quality and choose optimal parameters, in this subsection, we plot the PSNRs curve and FSIMs curve for our proposed algorithm versus μ and c respectively. For the penalty factor parameter, we empirically choose $\mu \in [10^{-6}, 1]$, where we fix other parameters and then evaluate the PSNRs and FSIMs. We choose the typical image ‘House’ to carry out the experiments under three different sampling rates of 0.2, 0.3 and 0.4. Figure 1 (a) and (b) present the PSNRs curve and FSIMs curve respectively, from the results we can observe that our proposed algorithm can obtain the best reconstruction quality when $\mu \in (10^{-3} \sim 10^{-1})$ for all the measurements.

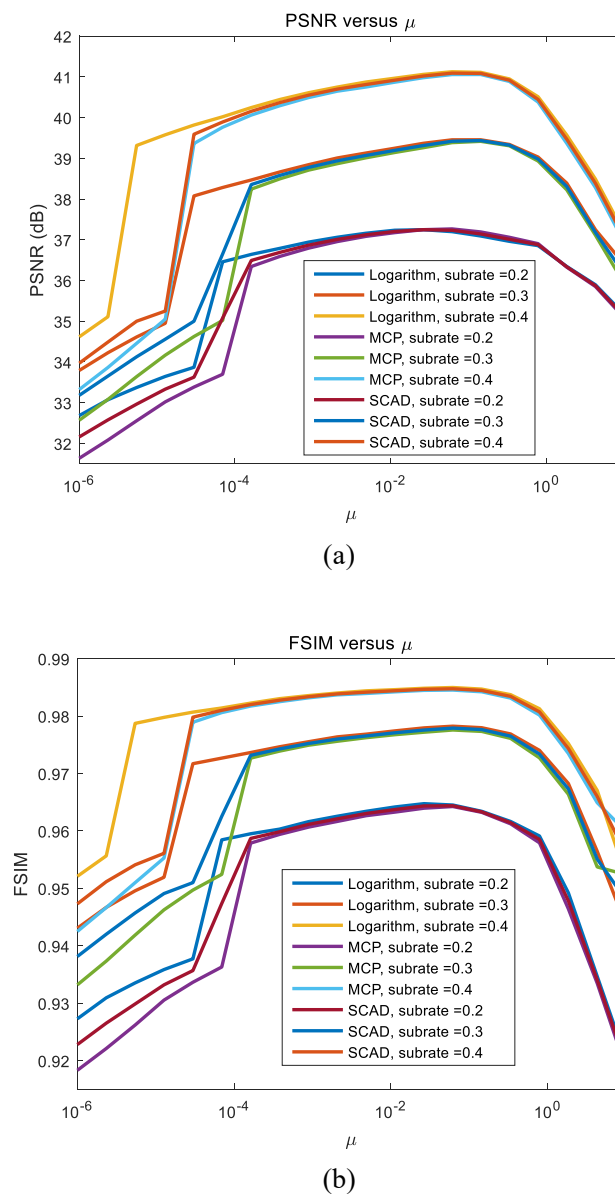
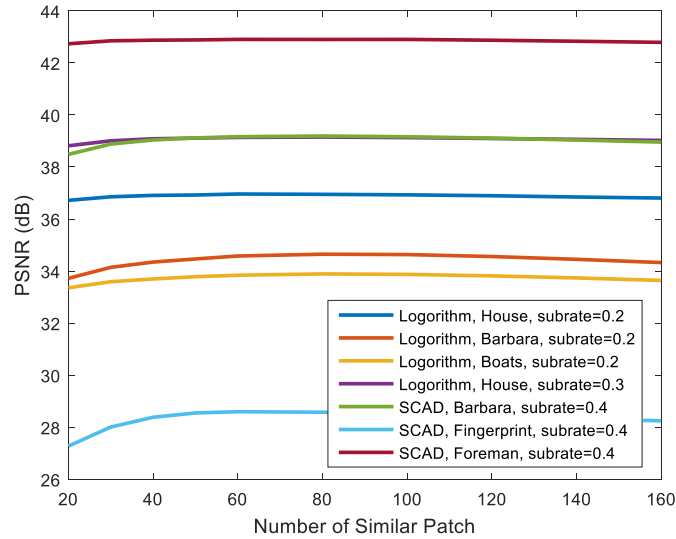
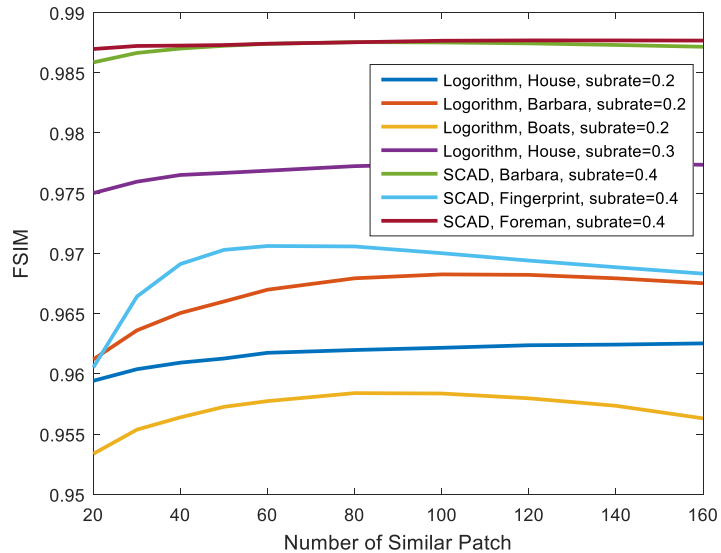


Figure 2. Performance of compressive sensing reconstruction for 0.1, 0.2 and 0.3 measurements of ‘House’. (a) PSNR versus the parameter μ ; (b) FSIM versus the parameter μ .

For the best match parameter c , we conduct experiment employ the surrogate functions of Logarithm and SCAD employ several typical images for experiments, and we fix the sampling rate to be 0.2, 0.3 and 0.4 for Logarithm function and SCAD function. Figure 3 (a) and (b) plot the PSNRs curve and the FSIMs curve versus c , from the results we can also observe that the proposed algorithm is not sensitive to the parameter c , and can achieve the favorable PSNRs and FSIMs when the $c \in [60,100]$, however, we empirically find that a larger c will bring higher computational time cost. Hence, in this paper, we set $c = 60$ for all our following experiments.



(a)



(b)

Figure 3. Performance of compressive sensing reconstruction for three different images of 'House', 'Barbara' and 'Boats'. (a) PSNR versus the number of similar patch c ; (b) FSIM versus the number of similar patch c ;

Table 1 presents the important parameters setting for five penalty functions under different sub-rates for our experiments.

Table 1 The parameter selections for five penalty functions under different sub-rates

Different penalties	0.1	0.2	0.3	0.4	0.5
$L_p (\mu, p)$	(0.0010, 0.6)	(0.0010, 0.6)	(0.0050, 0.6)	(0.0250, 0.6)	(0.0750, 0.6)
Logarithm (μ, γ)	(0.0100, 10^{-2})	(0.0001, 10^{-2})	(0.0050, 10^{-2})	(0.0250, 10^{-2})	(0.0750, 10^{-2})
MCP (μ, γ)	(0.0050, 10^6)	(0.0005, 10^2)	(0.0010, 10^2)	(0.0250, 10^2)	(0.0750, 10^2)
SCAD (μ, γ)	(0.0100, 10^6)	(0.0010, 10^6)	(0.0050, 10^6)	(0.0250, 10^6)	(0.1000, 10^6)
ETP (μ, γ)	(0.0010, 10^{-2})	(0.0010, 10^{-2})	(0.0050, 10^{-2})	(0.0250, 10^{-2})	(0.0750, 10^{-2})

4.2 Effect comparison with the nonconvex weighted strategy

4.2.1 Effect comparison with the nonconvex strategy

To evaluate the effect of our proposed nonconvex strategy, this subsection will conduct comparative experiments between the convex weighted model (Weighted NNM) and our proposed nonconvex weighted model, we employ the popular Logarithm function as the case and reconstructing a ‘Barbara’ image from 20%, 30% and 40% under-sampled data. Figure 4 present the PSNR curves comparisons versus the iteration number, we can find that our proposed nonconvex strategy can improve the corresponding weighted NNM based model significantly.

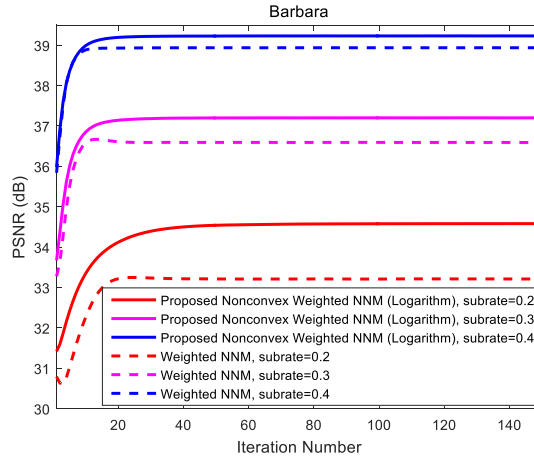


Figure 4. PSNR curves comparisons versus the iteration number between the weighted NNM and our proposed nonconvex weighted NNM model (Logarithm).

4.2.2 Effect comparison with the weighting strategy

To evaluate the effect of our proposed weighted strategy, this subsection will conduct comparative experiments between the nonconvex NNM model without weighting strategy and our proposed nonconvex weighted model, we employ the popular Logarithm function as the case and reconstructing a ‘House’ image from 20%, 30% and 40% under-sampled data. Figure 5 present the PSNR curves comparisons versus the iteration number, we can find that our proposed weighting strategy can outperform the corresponding nonconvex NNM based model without weighting strategy significantly.

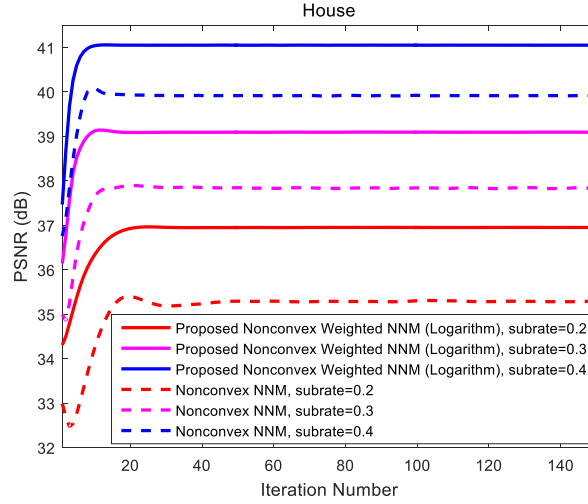


Figure 5. PSNR curves comparisons versus the iteration number between the nonconvex NNM and our proposed nonconvex weighted NNM model (Logarithm).

4.3 Convergence analysis

Although the nonconvex penalized regularization model can obtain better performance than the convex surrogate, it is tractable to demonstrate the convergence of our proposed algorithm. In this subsection, we will present the convergence property of our proposed algorithm visually by the PSNR curve versus the iteration number. Figure 4 (a) (b) (c) and (d) (e) present the PSNRs curves for L_p function, Logarithm function, MCP function, SCAD function and ETP function under different sub-sampling rates, from the results shown in figure 6 (a)-(e), we can observe that our proposed algorithm for the nonconvex framework contains good convergence property.

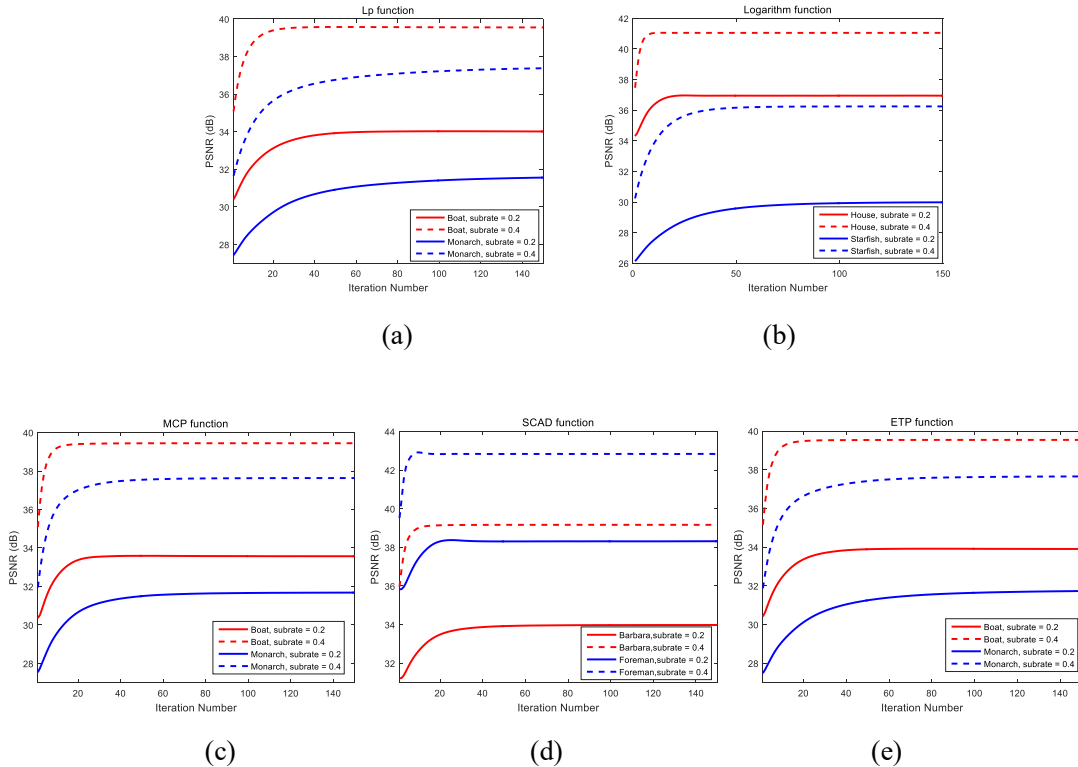


Figure 6 The convergence of the proposed algorithm for Logarithm function, MCP function and SCAD function with different rates of 0.2 and 0.4.

4.4 Comparisons with state-of-the art approaches

To demonstrate the effectiveness of our proposed algorithm, we employ four representative convex compressive sensing recovery algorithms for comparisons, include the algorithms of BCS [48], SGSR [49], ALSB [50] and JASR [51]. The selection of (μ, γ) is list in the table I for different sub-sampling rate and surrogate functions. Table II and III list the PSNR and FSIM of four convex state-of-the art algorithms and our proposed nonconvex algorithm under five different sampling rate of 0.1, 0.2, 0.3, 0.4 and 0.5. Without loss of generality, we employ three different penalty functions of MCP, SCAD and Logarithm as surrogates, respectively. We can observe that our proposed nonconvex weighted Group-prior model can obtain higher PSNR values and FSIM values.

Table II The PSNR comparisons of proposed algorithm and other state-of-the art algorithms

Rate	Method	Barbara	Boats	Elaine	Fingerprint	Foreman	House	Leaves	Monarch	Starfish
10%	BCS	22.80	24.52	27.46	17.15	29.76	26.90	18.54	21.70	22.71
	SGSR	28.70	27.71	31.32	20.47	34.88	32.77	22.22	24.27	22.91
	ALSB	27.01	27.75	30.99	20.64	33.49	32.18	21.37	24.27	23.63
	JASR	29.58	28.59	32.01	21.04	35.61	33.49	23.62	25.83	24.39
	Proposed (MCP)	29.84	28.55	32.31	20.77	36.12	33.99	24.32	26.27	25.49
	Proposed (SCAD)	29.91	28.70	31.48	20.95	36.15	34.07	24.96	26.86	24.90
	Proposed (logarithm)	29.89	28.81	32.36	21.07	36.10	34.11	25.20	27.06	25.13
20%	BCS	24.31	27.05	31.19	18.55	32.88	30.58	21.24	25.21	25.27
	SGSR	33.45	32.41	34.86	23.60	36.98	35.81	28.74	28.76	27.19
	ALSB	31.77	33.04	35.11	23.49	35.33	35.93	27.14	28.39	27.20
	JASR	34.16	33.21	35.66	23.98	37.87	36.10	30.24	30.60	29.10
	Proposed (MCP)	34.25	33.59	35.81	24.27	38.53	36.82	31.44	31.68	29.89
	Proposed (SCAD)	34.46	33.65	35.87	23.74	38.68	37.00	31.30	31.56	29.73
	Proposed (logarithm)	34.58	33.84	36.06	24.18	38.66	36.96	30.88	31.80	30.00
30%	BCS	25.70	28.93	33.70	20.05	35.16	32.87	23.31	27.70	27.17
	SGSR	35.91	35.22	36.87	25.84	38.47	37.37	32.98	31.99	30.79
	ALSB	34.70	36.45	37.49	25.85	36.50	38.36	31.30	31.37	30.43
	JASR	36.59	36.08	36.83	26.21	38.54	38.04	33.70	33.63	32.33
	Proposed (MCP)	37.07	36.86	38.19	26.52	40.93	39.02	35.12	34.82	33.27
	Proposed (SCAD)	37.16	37.09	38.09	26.15	41.14	39.41	34.84	34.51	32.93
	Proposed (logarithm)	37.20	37.04	38.28	26.44	41.02	39.14	35.19	34.89	33.39
40%	BCS	27.19	30.60	35.70	21.71	37.04	34.67	25.23	29.75	28.97
	SGSR	37.70	37.41	38.63	27.85	39.84	38.99	35.83	34.66	33.66
	ALSB	37.23	38.88	39.48	27.67	42.62	40.06	34.47	34.52	33.24
	JASR	37.39	37.19	38.28	28.26	41.19	38.79	36.56	36.15	34.30
	Proposed (MCP)	39.16	39.44	40.08	28.60	42.90	40.97	38.49	37.63	36.16
	Proposed (SCAD)	39.21	39.50	40.01	28.14	43.12	41.14	38.57	37.63	36.16
	Proposed (logarithm)	39.23	39.52	40.12	28.50	42.99	41.06	38.60	37.67	36.24

50%	BCS	28.79	32.24	37.52	23.56	38.79	36.37	27.03	31.79	30.72
	SGSR	39.38	39.30	40.08	30.00	41.15	40.56	38.19	36.99	35.88
	ALSB	39.44	40.93	41.19	29.67	44.40	41.80	37.67	36.99	36.09
	JASR	40.31	40.30	39.47	30.18	42.69	41.44	39.06	38.36	37.14
	Proposed (MCP)	41.04	41.44	41.69	30.66	44.54	42.50	41.23	40.15	38.48
	Proposed (SCAD)	41.05	41.47	41.65	30.44	44.78	42.64	41.38	40.14	38.48
	Proposed (logarithm)	41.08	41.49	41.72	30.62	44.66	42.57	41.33	40.21	38.53

Table III The FSIM comparisons of proposed algorithm and other state-of-the art algorithms

Rate	Method	Barbara	Boats	Elaine	Fingerprint	Foreman	House	Leaves	Monarch	Starfish
10%	BCS	0.7891	0.8029	0.8811	0.6165	0.8911	0.8455	0.6852	0.7828	0.8049
	SGSR	0.9147	0.8915	0.9220	0.8655	0.9393	0.9187	0.8356	0.8371	0.8177
	ALSB	0.8903	0.8830	0.9184	0.8651	0.9254	0.9069	0.7934	0.8218	0.8343
	JASR	0.9223	0.9035	0.9282	0.8722	0.9437	0.9167	0.8799	0.8822	0.8516
	Proposed (MCP)	0.9280	0.9047	0.9323	0.8742	0.9510	0.9285	0.8999	0.8910	0.8751
	Proposed (SCAD)	0.9281	0.9058	0.9268	0.8765	0.9512	0.9100	0.8578	0.9007	0.8697
	Proposed (logarithm)	0.9270	0.9061	0.9319	0.8775	0.9509	0.9301	0.9123	0.9044	0.8740
20%	BCS	0.8429	0.8640	0.9280	0.7378	0.9296	0.9014	0.7567	0.8465	0.8616
	SGSR	0.9615	0.9465	0.9551	0.9208	0.9598	0.9502	0.9373	0.9132	0.8993
	ALSB	0.9501	0.9512	0.9597	0.9200	0.9460	0.9541	0.9094	0.8965	0.8973
	JASR	0.9651	0.9521	0.9603	0.9256	0.9636	0.9425	0.9516	0.9409	0.9295
	Proposed (MCP)	0.9648	0.9047	0.9622	0.9280	0.9696	0.9608	0.9607	0.9498	0.9378
	Proposed (SCAD)	0.9677	0.9569	0.9646	0.9237	0.9710	0.9651	0.9563	0.9488	0.9358
	Proposed (logarithm)	0.9670	0.9577	0.9638	0.9286	0.9702	0.9617	0.9615	0.9506	0.9399
30%	BCS	0.8780	0.8995	0.9512	0.8191	0.9504	0.9298	0.8062	0.8839	0.8954
	SGSR	0.9762	0.9684	0.9695	0.9481	0.9711	0.9648	0.9676	0.9469	0.9447
	ALSB	0.9716	0.9744	0.9742	0.9487	0.9575	0.9730	0.9537	0.9296	0.9412
	JASR	0.9785	0.9723	0.9661	0.9510	0.9649	0.9649	0.9719	0.9610	0.9580
	Proposed (MCP)	0.9804	0.9558	0.9765	0.9545	0.9812	0.9763	0.9792	0.9677	0.9641
	Proposed (SCAD)	0.9815	0.9772	0.9767	0.9517	0.9822	0.9791	0.9794	0.9666	0.9617
	Proposed (logarithm)	0.9810	0.9771	0.9769	0.9541	0.9815	0.9769	0.9797	0.9677	0.9652
40%	BCS	0.9069	0.9246	0.9656	0.8776	0.9646	0.9491	0.8459	0.9115	0.9213
	SGSR	0.9835	0.9793	0.9784	0.9653	0.9788	0.9759	0.9799	0.9648	0.9661
	ALSB	0.9830	0.9838	0.9830	0.9643	0.9871	0.9820	0.9730	0.9581	0.9642
	JASR	0.9803	0.9764	0.9742	0.9679	0.9808	0.9676	0.9831	0.9739	0.9677
	Proposed (MCP)	0.9874	0.9764	0.9842	0.9706	0.9874	0.9845	0.9889	0.9793	0.9788
	Proposed (SCAD)	0.9875	0.9859	0.9843	0.9678	0.9881	0.9856	0.9893	0.9793	0.9788
	Proposed (logarithm)	0.9876	0.9860	0.9845	0.9700	0.9876	0.9848	0.9892	0.9793	0.9792
50%	BCS	0.9308	0.9438	0.9757	0.9192	0.9748	0.9638	0.8783	0.9343	0.9413
	SGSR	0.9885	0.9855	0.9844	0.9778	0.9844	0.9832	0.9872	0.9762	0.9772
	ALSB	0.9891	0.9896	0.9883	0.9754	0.9912	0.9882	0.9854	0.9740	0.9786
	JASR	0.9902	0.9881	0.9798	0.9789	0.9865	0.9848	0.9895	0.9818	0.9823

Proposed (MCP)	0.9916	0.9857	0.9889	0.9813	0.9907	0.9890	0.9934	0.9863	0.9862
Proposed (SCAD)	0.9918	0.9905	0.9890	0.9802	0.9915	0.9898	0.9936	0.9863	0.9862
Proposed (logarithm)	0.9917	0.9905	0.9890	0.9811	0.9912	0.9894	0.9935	0.9864	0.9864

To make a visual comparison, we choose three typical images of boats, leaves and monarch for 0.1 measurements, and choose fingerprint and leaves for 0.2 measurements, and the reconstructed results are presented in the figure 7, 8, 9, 10 and 11. It can be observed that our proposed algorithm can reconstruct images with higher quality.

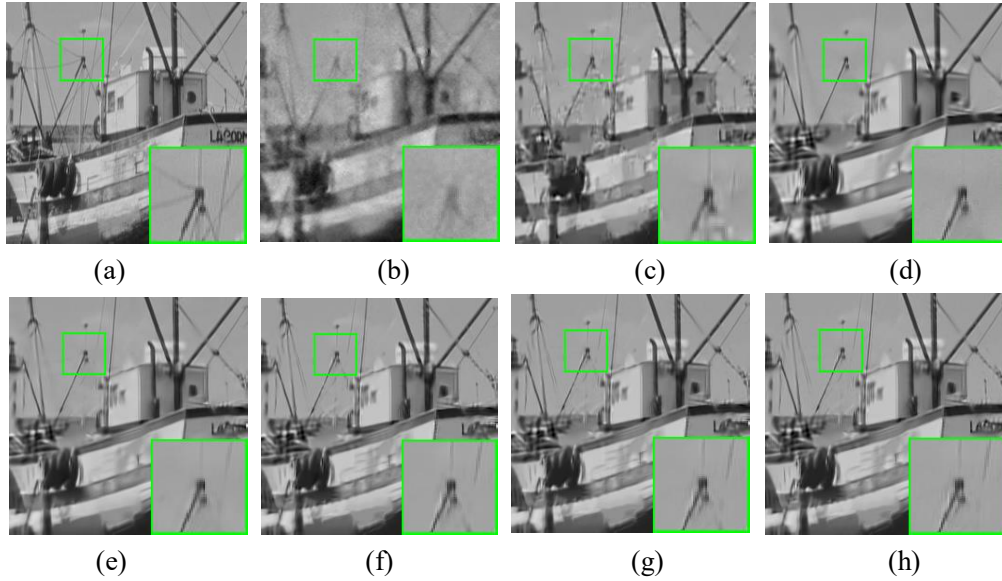


Figure 7. Visual comparison of the original image and seven reconstructed images by BCS, ALSB, ALSB, GSR, JASR and our proposed algorithms for 0.1 measurements of boats.

(a) Original Image; (b) SBCS, 24.52 dB; (c) ALSB, 27.75 dB; (d) SGSR, 27.71 dB; (e) JASR, 28.59 dB; (f) Proposed (MCP), 28.55 dB; (g) Proposed (SCAD), 28.70 dB; (h) Proposed (Logarithm), 28.81 dB;

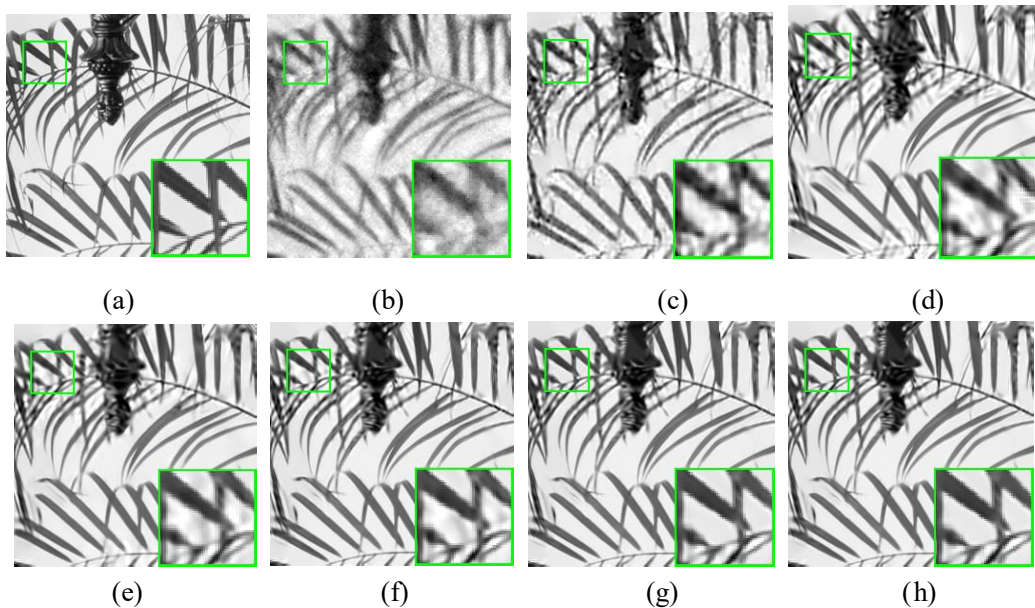


Figure 8. Visual comparison of the original image and seven reconstructed images by BCS, ALSB, ALSB, SGSR, JASR and our proposed algorithms for 0.1 measurements of leaves.

(a) Original Image; (b) BCS, 18.54 dB; (c) ALSB, 21.37 dB; (d) SGSR, 22.22;
(e) JASR, 23.62 dB; (f) Proposed (MCP) 24.32 dB; (g) Proposed (SCAD) 24.96 dB; (h) Proposed (Logarithm), 25.20 dB;

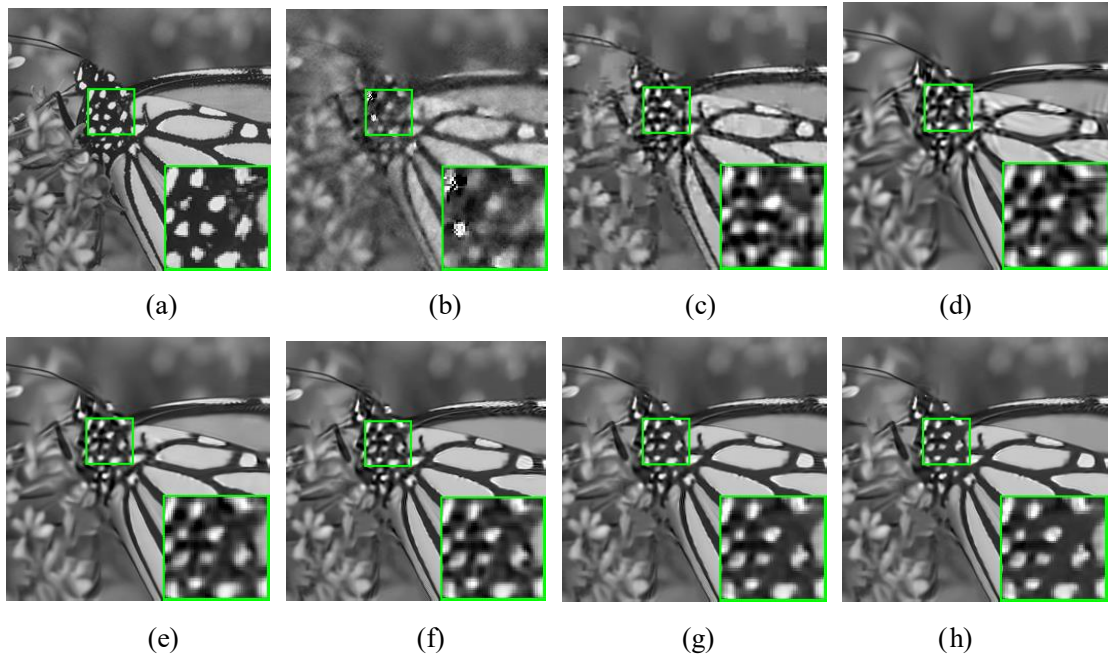
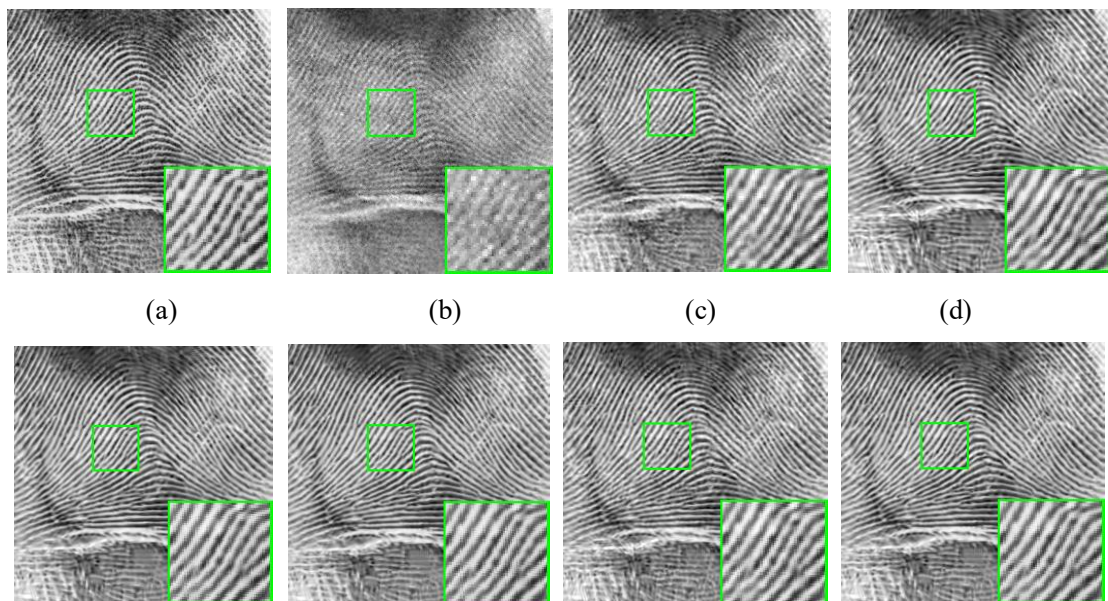


Figure 9. Visual comparison of the original image and five reconstructed images by BCS, ALSB, ALSB, GSR, JASR and our proposed algorithms for 0.1 measurements of monarch.

(a) Original Image; (b) SBCS, 21.70 dB; (c) ALSB, 24.27 dB; (d) SGSR, 24.27 dB; (e) JASR, 25.83 dB; (f) Proposed (MCP), 26.27; (g) Proposed (SCAD), 26.86 dB; (h) Proposed (Logarithm), 27.06 dB;



(e) (f) (g) (h)

Figure 10. Visual comparison of the original image and five reconstructed images by BCS, ALSB, ALSB, GSR, JASR and our proposed algorithms for 0.2 measurements of fingerprint.

(a) Original Image; (b) SBCS, 18.55 dB; (c) ALSB, 23.49 dB; (d) SGSR, 23.60;
(e) JASR, 23.98 dB; (f) Proposed (MCP), 24.27 dB; (g) Proposed (SCAD), 23.74 dB;
(h) Proposed (Logarithm), 24.18 dB;

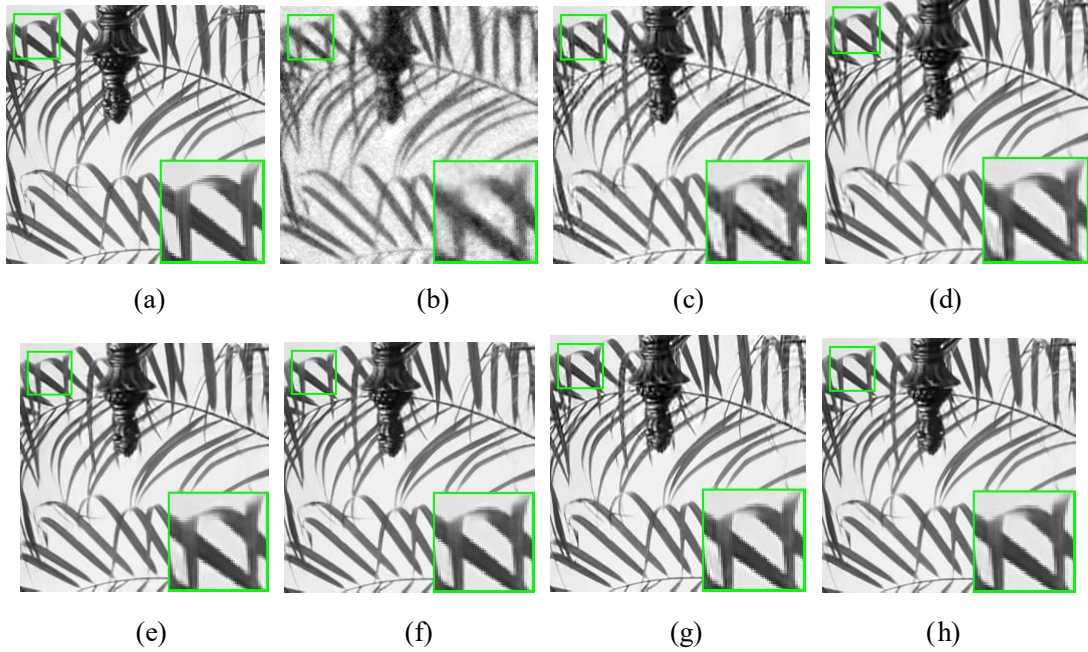


Figure 11. Visual comparison of the original image and five reconstructed images by BCS, ALSB, ALSB, SGSR, JASR and our proposed algorithms for 0.2 measurements of leaves.

(a) Original Image; (b) SBCS, 21.24 dB; (c) ALSB, 27.14 dB; (d) SGSR, 28.74;
(e) JASR, 30.24 dB; (f) Proposed (MCP), 31.44 dB; (g) Proposed (SCAD), 31.30 dB;
(h) Proposed (Logarithm), 30.88 dB;

5. Conclusion

This paper targeted at compressive sensing image reconstruction by applying the nonconvex surrogate of L_0 -norm on the singular values to approximate the group sparse representation (GSR) based low-rank function, and utilized the typical Logarithm function to regularize the sparsity. To solve the resulting optimization problem, we propose an iteratively reweighted NNM algorithm based on the ADMM framework. Considering the fact that the regularization parameter plays a crucial role for the reconstruction quality, we employ an adaptive scheme to make the tradeoff between the fidelity term and the regularizer. Experimental results show that our proposed algorithm can enhance the low-rank matrix recovery compared with the state-of-the-art convex algorithms.

Acknowledge

The authors would like to thank Associate Editor for his efforts in coordinating the review of our manuscript, and thank three anonymous reviewers for their constructive suggestions to improve the manuscript. We also express our gratitude to Dr. Zhiyuan Zha for providing the source code.

Reference

- [1] E.J. Candes, M.B. Wakin, An Introduction To Compressive Sampling, *IEEE Signal Process. Mag.* 25 (2008) 21–30. doi:10.1109/MSP.2007.914731.
- [2] L.C. Potter, E. Ertin, J.T. Parker, M. Çetin, Sparsity and compressed sensing in radar imaging, *Proc. IEEE.* 98 (2010) 1006–1020. doi:10.1109/JPROC.2009.2037526.
- [3] H. Bu, R. Tao, X. Bai, J. Zhao, Regularized smoothed L0 norm algorithm and its application to CS-based radar imaging, *Signal Processing.* 122 (2016) 115–122. doi:10.1016/j.sigpro.2015.11.024.
- [4] G. Gui, L. Xu, S. Matsushita, Improved adaptive sparse channel estimation using mixed square/fourth error criterion, *J. Franklin Inst.* 352 (2015) 4579–4594. doi:10.1016/j.jfranklin.2015.07.006.
- [5] G. Gui, N. Liu, L. Xu, F. Adachi, Low-complexity large-scale multiple-input multiple-output channel estimation using affine combination of sparse least mean square filters, *IET Commun.* 9 (2015) 2168–2175. doi:10.1049/iet-com.2014.0979.
- [6] D.S. Owodunni, A. Ali, A.A. Quadeer, E.B. Al-Safadi, O. Hammi, T.Y. Al-Naffouri, Compressed sensing techniques for receiver based post-compensation of transmitter’s nonlinear distortions in OFDM systems, *Signal Processing.* 97 (2014) 282–293. doi:10.1016/j.sigpro.2013.10.029.
- [7] G. Gui, H. Huang, Y. Song, H. Sari, Deep Learning for an Effective Nonorthogonal Multiple Access Scheme, *IEEE Trans. Veh. Technol.* 67 (2018) 8440–8450. doi:10.1109/TVT.2018.2848294.
- [8] H. Huang, J. Yang, Y. Song, H. Huang, G. Gui, Deep Learning for Super-Resolution Channel Estimation and DOA Estimation based Massive MIMO System, *IEEE Trans. Veh. Technol.* 67 (2018) 8549–8560. doi:10.1109/TVT.2018.2851783.
- [9] B. Liu, G. Gui, S. Matsushita, L. Xu, Dimension-reduced direction-of-arrival estimation based on L2,1-norm penalty, *IEEE Access.* 6 (2018) 44433–44444.
- [10] F. Wen, P. Liu, Y. Liu, R.C. Qiu, W. Yu, Robust sparse recovery in impulsive noise via Lp-L1 Optimization, *IEEE Trans. Signal Process.* 65 (2017) 105–118.
- [11] X. Li, Z. Sun, W. Yi, G. Cui, L. Kong, X. Yang, Computationally efficient coherent detection and parameter estimation algorithm for maneuvering target, *Signal Processing.* 155 (2019) 130–142. doi:10.1016/j.sigpro.2018.09.030.
- [12] J. Wen, Z. Zhou, Z. Liu, M.J. Lai, X. Tang, Sharp sufficient conditions for stable recovery of block sparse signals by block orthogonal matching pursuit, *Appl. Comput. Harmon. Anal.* (2018) 1–27. doi:10.1016/j.acha.2018.02.002.
- [13] J. Wen, Z. Zhou, D. Li, X. Tang, A novel sufficient condition for generalized orthogonal matching pursuit, *IEEE Commun. Lett.* 21 (2017) 805–808. doi:10.1109/LCOMM.2016.2642922.

- [14] J. Zhang, Z.L. Yu, Z. Gu, Y. Li, Z. Lin, Multichannel Electrocardiogram Reconstruction in Wireless Body Sensor Networks Through Weighted L_{1,2} Minimization, *IEEE Trans. Instrum. Meas.* 67 (2018) 2024–2034. doi:10.1109/TIM.2018.2811438.
- [15] J. Cheng, S. Jia, L. Ying, Y. Liu, S. Wang, Y. Zhu, Y. Li, C. Zou, X. Liu, D. Liang, Improved parallel image reconstruction using feature refinement, *Magn. Reson. Med.* 80 (2018) 211–223. doi:10.1002/mrm.27024.
- [16] S. Wang, S. Tan, Y. Gao, Q. Liu, L. Ying, T. Xiao, Y. Liu, X. Liu, H. Zheng, D. Liang, Learning Joint-Sparse Codes for Calibration-Free Parallel MR Imaging, *IEEE Trans. Med. Imaging.* 37 (2018) 251–261. doi:10.1109/TMI.2017.2746086.
- [17] D. Liang, E.V.R. DiBella, R.R. Chen, L. Ying, K-t ISD: Dynamic cardiac MR imaging using compressed sensing with iterative support detection, *Magn. Reson. Med.* 68 (2012) 41–53. doi:10.1002/mrm.23197.
- [18] Z. Zha, X. Liu, X. Huang, H. Shi, Y. Xu, Q. Wang, L. Tang, X. Zhang, Analyzing the group sparsity based on the rank minimization methods, in: *IEEE Int. Conf. Multimed. Expo, 2017*: pp. 883–888. doi:10.1109/ICME.2017.8019334.
- [19] Y. Li, S. Fan, J. Yang, J. Xiong, X. Cheng, G. Gui, S. Hikmet, MUSAI-L1/2: Multiple Sub-wavelet-dictionaries-based Adaptively-weighted Iterative Half Thresholding Algorithm for Compressive Imaging, *IEEE Access.* 6 (2018) 16795–16805. doi:10.1109/ACCESS.2018.2799984.
- [20] Y. Li, F. Dai, X. Cheng, L. Xu, G. Gui, Multiple-prespecified-dictionary sparse representation for compressive sensing image reconstruction with nonconvex regularization, *J. Franklin Inst.* 356 (2019) 2353–2371. doi:10.1016/j.jfranklin.2018.12.013.
- [21] A. Chambolle, An Algorithm for Total Variation Minimization and Applications, *J. Math. Imaging Vis.* 20 (2004) 89–97. doi:10.1023/B:JMIV.0000011321.19549.88.
- [22] A. Buades, B. Coll, J. Morel, A review of image denoising algorithms , with a new one To cite this version : HAL Id : hal-00271141, *Multiscale Model. Simul.* 4 (2005) 490–530.
- [23] K. Dabov, A. Foi, V. Katkovnik, K. Egiazarian, Image Denoising by Sparse 3-D Transform-Domain Collaborative Filtering, *IEEE Trans. Image Process.* 16 (2007) 2080–2095.
- [24] J. Yang, F. Liu, H. Yue, X. Fu, C. Hou, F. Wu, Textured Image Demoiréing via Signal Decomposition and Guided Filtering, *IEEE Trans. Image Process.* 26 (2017) 3528–3541.
- [25] H. Yue, X. Sun, S. Member, J. Yang, F. Wu, Image Denoising by Exploring External and Internal Correlations, *IEEE Trans. Image Process.* 24 (2015) 1967–1982. doi:10.1109/TIP.2015.2412373.
- [26] W. Dong, L. Zhang, G. Shi, X. Li, Nonlocally centralized sparse representation for image restoration, in: *IEEE Trans. Image Process.*, 2013: pp. 1620–1630. doi:10.1109/TIP.2012.2235847.
- [27] J. Zhang, D. Zhao, W. Gao, Group-Based Sparse Representation for Image Restoration, *Image Process. IEEE Trans.* 23 (2014) 3336–3351. doi:10.1109/TIP.2014.2323127.
- [28] Y. Li, Y. Lin, X. Cheng, Z. Xiao, F. Shu, G. Gui, Nonconvex Penalized Regularization for Robust Sparse Recovery in the Presence of S_αS Noise, *IEEE Access.* 6 (2018) 25474–25485. doi:10.1109/ACCESS.2018.2830771.
- [29] Y. Li, J. Zhang, S. Fan, J. Yang, J. Xiong, X. Cheng, H. Sari, F. Adachi, G. Gui, Sparse Adaptive Iteratively-Weighted Thresholding Algorithm (SAITA) for L_p-Regularization Using the Multiple Sub-Dictionary Representation, *Sensors.* 17 (2017) 2920–2936. doi:10.3390/s17122920.

- [30] I.E. Frank, J.H. Friedman, A Statistical of Some Chemometrics View Regression Tools, *Technometrics*. 35 (1993) 109–135. doi:10.2307/1269656.
- [31] Z. Xu, H. Zhang, Y. Wang, X. Chang, Y. Liang, $L_{\{1/2\}}$ Regularization: A Thersholding Representation Theory and a Fast Solver, *IEEE Tansactions Neural Netw. Learn. Syst.* 23 (2012) 1013–1027.
- [32] J. Fan, R. Li, Variable Selection via Nonconcave Penalized Likelihood and its Oracle Properties, *J. Am. Stat. Assoc.* 96 (2001) 1348–1360. doi:10.1198/016214501753382273.
- [33] J.H. Friedman, Fast sparse regression and classification, *Int. J. Forecast.* 28 (2012) 722–738. doi:10.1016/j.ijforecast.2012.05.001.
- [34] C.H. Zhang, Nearly unbiased variable selection under minimax concave penalty, 2010. doi:10.1214/09-AOS729.
- [35] J. Yang, X. Yang, X. Ye, C. Hou, Reconstruction of Structurally-Incomplete Matrices With Reweighted Low-Rank and Sparsity Priors, *IEEE Trans. Image Process.* 26 (2017) 1158–1172.
- [36] Y. Peng, J. Suo, Q. Dai, W. Xu, Reweighted Low-Rank Matrix Recovery and its Application in Image Restoration, *IEEE Trans. Cybern.* 44 (2014) 2418–2430. doi:10.1109/TCYB.2014.2307854.
- [37] W. Dong, G. Shi, X. Li, Y. Ma, F. Huang, Compressive sensing via nonlocal low-rank regularization, *IEEE Trans. Image Process.* 23 (2014) 3618–3632. doi:10.1109/TIP.2014.2329449.
- [38] Q. Wang, X. Zhang, Y. Wu, L. Tang, Z. Zha, Nonconvex Weighted ℓ_p Minimization Based Group Sparse Representation Framework for Image Denoising, *IEEE Signal Process. Lett.* 24 (2017) 1686–1690. doi:10.1109/LSP.2017.2731791.
- [39] J. Trzasko, A. Manduca, Highly undersampled magnetic resonance image reconstruction via homotopic L_0 -minimization, *IEEE Trans. Med. Imaging.* 28 (2009) 106–121. doi:10.1109/TMI.2008.927346.
- [40] C. Gao, N. Wang, A Feasible Nonconvex Relaxation Approach to Feature Selection, in: *Proc. Twenty-Fifth AAAI Conf. Artif. Intell.*, 2011: pp. 356–361.
- [41] J. Yang, Y. Zhang, Alternating direction algorithms for L_1 compressive sensing, *SIAM J. Sci. Comput.* 33 (2011) 250–278.
- [42] Z. Zha, X. Zhang, Y. Wu, Q. Wang, X. Liu, L. Tang, X. Yuan, Non-convex weighted ℓ_p nuclear norm based ADMM framework for image restoration, *Neurocomputing*. 311 (2018) 209–224. doi:10.1016/j.neucom.2018.05.073.
- [43] C. Lu, J. Tang, S. Yan, Z. Lin, Generalized nonconvex nonsmooth low-rank minimization, in: *Proc. IEEE Comput. Soc. Conf. Comput. Vis. Pattern Recognit.*, 2014: pp. 4130–4137. doi:10.1109/CVPR.2014.526.
- [44] K. Chen, H. Dong, K. Chan, Reduced rank regression via adaptive nuclear norm penalization, *Biometrika*. 100 (2013) 901–920. doi:10.1093/biomet/ast036.
- [45] E.J. Candes, M.B. Wakin, S.P. Boyd, Enhancing sparsity by reweighted L_1 minimization, *J. Fourier Anal. Appl.* 14 (2008) 877–905.
- [46] C. Chen, E.W. Tramel, J.E. Fowler, Compressed-sensing recovery of images and video using multihypothesis predictions, in: *2011 Conf. Rec. Forty Fifth Asilomar Conf. Signals, Syst. Comput.*, IEEE, 2011: pp. 1193–1198. doi:10.1109/ACSSC.2011.6190204.
- [47] L. Zhang, L. Zhang, X. Mou, D. Zhang, FSIM: A Feature Similarity Index for Image Quality Assessment, *IEEE Tansactions Image Process.* 20 (2011) 2378–2386.

- [48] Sungkwang Mun, J.E. Fowler, Block compressed sensing of images using directional transforms, in: Proc. Int. Conf. Image Process., 2009: pp. 3021–3024. doi:10.1109/ICIP.2009.5414429.
- [49] J. Zhang, D. Zhao, F. Jiang, W. Gao, Structural group sparse representation for image Compressive Sensing recovery, in: Data Compression Conf. Proc., IEEE, 2013: pp. 331–340. doi:10.1109/DCC.2013.41.
- [50] J. Zhang, C. Zhao, D. Zhao, W. Gao, Image compressive sensing recovery using adaptively learned sparsifying basis via L0 minimization, Signal Processing. 103 (2014) 114–126. doi:10.1016/j.sigpro.2013.09.025.
- [51] N. Eslahi, A. Aghagolzadeh, Compressive Sensing Image Restoration Using Adaptive Curvelet Thresholding and Nonlocal Sparse Regularization, IEEE Transactions Image Process. 25 (2016) 3126–3140.